

COULOMB GAUGE MODEL FOR EXOTIC HADRONS

STEPHEN R. COTANCH^a and FELIPE LLANES-ESTRADA^b^a*Department of Physics, North Carolina State University, Raleigh, NC 27695, USA*^b*Depto. Física Teórica I, Universidad Complutense de Madrid, 28040 Madrid, Spain*

Hadron structure advances provided by the Coulomb gauge model are summarized. Highlights include a realistic description of the vacuum and meson spectrum with chiral symmetry and dynamical flavor mixing, accurate hyperfine splittings for light and heavy systems, glueball and hybrid meson predictions in agreement with lattice QCD, and tetraquark results providing an understanding of the observed $\pi_1(1400)$ having unconventional quantum numbers.

PAC numbers: 11.30.Rd, 12.38.Lg, 12.39.Mk, 12.40.Vv, 12.40.Yx

Keywords: Coulomb gauge Hamiltonian, glueballs, hybrid mesons, tetraquarks

1. Introduction

Understanding whether exotic systems do or do not exist is one of the few remaining challenges for the Standard Model. Such states are those with explicit gluon, g , degrees of freedom and/or quarks, q , in color states that are not singlets. Hadrons with unconventional quantum numbers, i.e. those not possible in $q\bar{q}$ or qqq systems such as $J^{PC} = 1^{-+}$, may or may not be exotic. For example, one of the key predictions of the Coulomb gauge model described in this paper is that the observed 1^{-+} $\pi_1(1400)$ is not an exotic but rather a more conventional meson-meson resonance with quarks in two color singlet states. Addressing the above challenge has motivated the development and application of this model which provides a robust, relativistic field theoretical approach that retains the attractive, insightful wavefunction picture. Since QCD is intrinsically a non-perturbative many-body problem, an established, successful nuclear structure method has been adopted which entails three elements: 1) an effective Hamiltonian; 2) a truncated model space; 3) solving the equations of motion using standard many-body techniques. The Coulomb gauge model therefore uses several many-body techniques, Bardeen-Cooper-Schrieffer [BCS], Tamm-Dancoff [TDA], random phase approximation [RPA], coupled channels, variational and exact diagonalization to solve the equations of motion for an approximate QCD Hamiltonian in a model space spanned by a truncated number of particle Fock states. For this method to work the Fock space expansion, $|\Psi\rangle = |q\bar{q}\rangle + |gg\rangle + |q\bar{q}g\rangle + |q\bar{q}q\bar{q}\rangle + \dots$, must involve dressed (constituent) quaisparticle states, and not bare (current) quarks and gluons. This is because the dressed partons have much larger masses which, from energy considerations, enables a sensible truncation to describe the low mass hadron spectrum in analogy to the reasonable 1 particle-1 hole, 2 particle-2 hole, etc. truncations for low lying nuclear states.

The following sections detail the Coulomb gauge model beginning with the Hamiltonian in section 2 and the BCS vacuum treatment for dressing the bare

quarks and gluons in section 3. Applications to hadrons are discussed in section 4 for two-body $q\bar{q}$ (mesons) and gg (glueballs) states, section 5 for three-body ggg (oddballs) and $q\bar{q}g$ (hybrids) states, and section 6 for four-body $q\bar{q}q\bar{q}$ (tetraquarks) states. Section 6 also addresses dynamic mixing of two and four-body states. Finally, a summary is presented in section 7.

2. QCD Coulomb gauge model

In the Coulomb gauge the exact QCD Hamiltonian is

$$H_{\text{QCD}} = H_q + H_g + H_{qg} + H_C \quad (1)$$

$$H_q = \int d\mathbf{x} \Psi^\dagger(\mathbf{x}) [-i\boldsymbol{\alpha} \cdot \boldsymbol{\nabla} + \beta m] \Psi(\mathbf{x}) \quad (2)$$

$$H_g = \frac{1}{2} \int d\mathbf{x} [\mathcal{J}^{-1} \boldsymbol{\Pi}^a(\mathbf{x}) \cdot \mathcal{J} \boldsymbol{\Pi}^a(\mathbf{x}) + \mathbf{B}^a(\mathbf{x}) \cdot \mathbf{B}^a(\mathbf{x})] \quad (3)$$

$$H_{qg} = g \int d\mathbf{x} \mathbf{J}^a(\mathbf{x}) \cdot \mathbf{A}^a(\mathbf{x}) \quad (4)$$

$$H_C = -\frac{g^2}{2} \int d\mathbf{x} d\mathbf{y} \mathcal{J}^{-1} \rho^a(\mathbf{x}) K^{ab}(\mathbf{x}, \mathbf{y}) \mathcal{J} \rho^b(\mathbf{y}), \quad (5)$$

where g is the QCD coupling constant, Ψ is the quark field with current quark mass m , $A^a = (\mathbf{A}^a, A_0^a)$ are the gluon fields satisfying the transverse gauge condition, $\boldsymbol{\nabla} \cdot \mathbf{A}^a = 0$ ($a = 1, 2, \dots, 8$), $\boldsymbol{\Pi}^a = -\mathbf{E}_{tr}^a$ are the conjugate momenta,

$$\mathbf{E}_{tr}^a = -\dot{\mathbf{A}}^a + g(1 - \boldsymbol{\nabla}^{-2} \boldsymbol{\nabla} \boldsymbol{\nabla} \cdot) f^{abc} A_0^b \mathbf{A}^c \quad (6)$$

$$\mathbf{B}^a = \boldsymbol{\nabla} \times \mathbf{A}^a + \frac{1}{2} g f^{abc} \mathbf{A}^b \times \mathbf{A}^c, \quad (7)$$

are the non-abelian chromodynamic fields, $\mathbf{J}^a = \Psi^\dagger(\mathbf{x}) \boldsymbol{\alpha} T^a \Psi(\mathbf{x})$ are the quark currents, $\rho^a(\mathbf{x}) = \Psi^\dagger(\mathbf{x}) T^a \Psi(\mathbf{x}) + f^{abc} \mathbf{A}^b(\mathbf{x}) \cdot \boldsymbol{\Pi}^c(\mathbf{x})$ are the color densities with standard $SU(3)$ color matrices, $T^a = \frac{\lambda_a^a}{2}$, and structure constants, f^{abc} . The gauge manifold curvature is measured by the Faddeev-Popov determinant, $\mathcal{J} = \det(\mathcal{M})$, of the matrix, $\mathcal{M} = \boldsymbol{\nabla} \cdot \mathbf{D}$, with covariant derivative, $\mathbf{D}^{ab} = \delta^{ab} \boldsymbol{\nabla} - g f^{abc} \mathbf{A}^c$, which governs the kernel, $K^{ab}(\mathbf{x}, \mathbf{y}) = \langle \mathbf{x}, a | \mathcal{M}^{-1} \nabla^2 \mathcal{M}^{-1} | \mathbf{y}, b \rangle$. In this gauge, the color form of Gauss's law, which is essential for confinement, is satisfied exactly and can be used to eliminate the unphysical longitudinal gluon fields. The Hamiltonian is renormalizable, preserves rotational invariance, avoids spurious retardation corrections, aids identification of dominant, low energy potentials, permits resolution of the Gribov problem and has only physical degrees of freedom (no ghosts). The standard normal mode field expansions are (bare quark spinors u, v , helicity, $\lambda = \pm 1$, and color vectors $\hat{e}_{c=1,2,3}$)

$$\Psi(\mathbf{x}) = \int \frac{d\mathbf{k}}{(2\pi)^3} [u_\lambda(\mathbf{k}) b_{\lambda c}(\mathbf{k}) + v_\lambda(-\mathbf{k}) d_{\lambda c}^\dagger(-\mathbf{k})] e^{i\mathbf{k} \cdot \mathbf{x}} \hat{e}_c \quad (8)$$

$$\mathbf{A}^a(\mathbf{x}) = \int \frac{d\mathbf{k}}{(2\pi)^3} \frac{1}{\sqrt{2k}} [\mathbf{a}^a(\mathbf{k}) + \mathbf{a}^{a\dagger}(-\mathbf{k})] e^{i\mathbf{k} \cdot \mathbf{x}} \quad (9)$$

$$\boldsymbol{\Pi}^a(\mathbf{x}) = -i \int \frac{d\mathbf{k}}{(2\pi)^3} \sqrt{\frac{k}{2}} [\mathbf{a}^a(\mathbf{k}) - \mathbf{a}^{a\dagger}(-\mathbf{k})] e^{i\mathbf{k} \cdot \mathbf{x}}. \quad (10)$$

Here $b_{\lambda C}(\mathbf{k})$, $d_{\lambda C}(-\mathbf{k})$ and $a_{\mu}^a(\mathbf{k})$ ($\mu = 0, \pm 1$) are the respective quark, anti-quark and gluon Fock operators, the latter satisfying the transverse commutation relations

$$\begin{aligned} [a_{\mu}^a(\mathbf{k}), a_{\mu'}^{b\dagger}(\mathbf{k}')] &= (2\pi)^3 \delta_{ab} \delta^3(\mathbf{k} - \mathbf{k}') [\delta_{\mu\mu'} - (-1)^{\mu} \frac{k_{\mu} k_{-\mu'}}{k^2}] \\ &= (2\pi)^3 \delta_{ab} \delta^3(\mathbf{k} - \mathbf{k}') D_{\mu\mu'}(\mathbf{k}) , \end{aligned} \quad (11)$$

due to the Coulomb gauge condition, $\mathbf{k} \cdot \mathbf{a}^a(\mathbf{k}) = (-1)^{\mu} k_{\mu} a_{-\mu}^a(\mathbf{k}) = 0$.

The Coulomb gauge model Hamiltonian, H_{CG} , is obtained by replacing the Coulomb kernel with a calculable confining potential and using the lowest order, unit value for the the Faddeev-Popov determinant

$$H_{CG} = H_q + H_g^{\text{CG}} + H_{qg}^{\text{CG}} + H_C^{\text{CG}} \quad (12)$$

$$H_g^{\text{CG}} = \frac{1}{2} \int d\mathbf{x} [\mathbf{\Pi}^a(\mathbf{x}) \cdot \mathbf{\Pi}^a(\mathbf{x}) + \mathbf{B}^a(\mathbf{x}) \cdot \mathbf{B}^a(\mathbf{x})] \quad (13)$$

$$H_{qg}^{\text{CG}} = \frac{1}{2} \int d\mathbf{x} d\mathbf{y} J_i^a(\mathbf{x}) \left(\delta_{ij} - \frac{\nabla_i \nabla_j}{\nabla^2} \right)_{\mathbf{x}} U(|\mathbf{x} - \mathbf{y}|) J_j^a(\mathbf{y}) \quad (14)$$

$$H_C^{\text{CG}} = -\frac{1}{2} \int d\mathbf{x} d\mathbf{y} \rho^a(\mathbf{x}) V(|\mathbf{x} - \mathbf{y}|) \rho^a(\mathbf{y}) . \quad (15)$$

Also, using Maxwell's equation, the quark-gluon Hamiltonian has been converted to a quark-quark hyperfine interaction involving an effective massive ($m_g = 600$ MeV) gluon exchange potential (modified Yukawa kernel)

$$U(p) = \left\{ \begin{array}{ll} -\frac{8.07}{p^2} \frac{\ln^{-0.62}(\frac{p^2}{m_g^2} + 0.82)}{\ln^{0.8}(\frac{p^2}{m_g^2} + 1.41)} & p > m_g \\ -\frac{5.509}{p^2 + m_g^2} & p < m_g \end{array} \right\} . \quad (16)$$

Confinement is provided by the Cornell potential, $V(r) = -\alpha_s/r + \sigma r$, or in momentum space, $V(p) = -4\pi\alpha_s/p^2 - 8\pi\sigma/p^4$. The string tension, $\sigma = 0.135$ GeV², and $\alpha_s = 0.4$ have been independently determined and set the scale for the calculation. The remaining parameters are the bare (current) quark masses, $m_u = m_d = 5$ MeV, $m_s = 80$ MeV, $m_c = 640$ MeV and $m_b = 3.33$ GeV.

3. BCS vacuum and gap equations

The Bardeen-Cooper-Schriber method is used to obtain the ground state (vacuum). This entails rotating the field operators

$$\begin{aligned}
B_{\lambda C}(\mathbf{k}) &= \cos \frac{\theta_k}{2} b_{\lambda C}(\mathbf{k}) - \lambda \sin \frac{\theta_k}{2} d_{\lambda C}^\dagger(-\mathbf{k}) \\
D_{\lambda C}(-\mathbf{k}) &= \cos \frac{\theta_k}{2} d_{\lambda C}(-\mathbf{k}) + \lambda \sin \frac{\theta_k}{2} b_{\lambda C}^\dagger(\mathbf{k}) \\
\alpha^a(\mathbf{k}) &= \cosh \Theta_k \mathbf{a}^a(\mathbf{k}) + \sinh \Theta_k \mathbf{a}^{a\dagger}(-\mathbf{k}) ,
\end{aligned} \tag{17}$$

producing the dressed, quasi-particle operators α^a , $B_{\lambda C}$ and $D_{\lambda C}$. The BCS quasi-particle vacuum, $|\Omega\rangle$, is defined by $B_{\lambda C}|\Omega\rangle = D_{\lambda C}|\Omega\rangle = \alpha_\mu^a|\Omega\rangle = 0$, and builds on the bare parton vacuum, $|0\rangle$, $b_{\lambda C}|0\rangle = d_{\lambda C}|0\rangle = a_\mu^a|0\rangle = 0$,

$$|\Omega_{quark}\rangle = [e^{-\int \frac{d\mathbf{k}}{(2\pi)^3} \lambda \tan \frac{\theta_k}{2} b_{\lambda C}^\dagger(\mathbf{k}) d_{\lambda C}^\dagger(-\mathbf{k})}] |0\rangle \tag{18}$$

$$|\Omega_{gluon}\rangle = [e^{-\int \frac{d\mathbf{k}}{(2\pi)^3} \frac{1}{2} \tanh \Theta_k D_{\mu\mu'}(\mathbf{k}) a_\mu^{a\dagger}(\mathbf{k}) a_{\mu'}^{a\dagger}(-\mathbf{k})}] |0\rangle . \tag{19}$$

Quark and gluon condensates (correlated $q\bar{q}$ and gg Cooper pairs) naturally emerge in the composite BCS vacuum, $|\Omega\rangle = |\Omega_{quark}\rangle \otimes |\Omega_{gluon}\rangle$. A variational minimization of the model ground state, $\delta\langle\Omega|H_{CG}|\Omega\rangle = 0$, yields the constituent quark and gluon gap equations

$$\begin{aligned}
k s_k - m_q c_k &= \frac{2}{3} \int \frac{d\mathbf{q}}{(2\pi)^3} [V(|\mathbf{k} - \mathbf{q}|)(s_k c_q x - s_q c_k) \\
&\quad - 4(c_k s_q U(|\mathbf{k} - \mathbf{q}|) - c_q s_k W(|\mathbf{k} - \mathbf{q}|))] \tag{20}
\end{aligned}$$

$$W(|\mathbf{k} - \mathbf{q}|) \equiv U(|\mathbf{k} - \mathbf{q}|) \frac{x(k^2 + q^2) - qk(1 + x^2)}{|\mathbf{k} - \mathbf{q}|^2} \tag{21}$$

$$\omega_k^2 = k^2 - \frac{3}{4} \int \frac{d\mathbf{q}}{(2\pi)^3} [V(|\mathbf{k} - \mathbf{q}|) \frac{(1 + x^2)(\omega_q^2 - \omega_k^2)}{\omega_q} - g^2 \frac{(1 - x^2)}{\omega_q}] , \tag{22}$$

with $s_k = \sin\phi_k$, $c_k = \cos\phi_k$ and $x = \mathbf{k} \cdot \mathbf{q}$. Here $\phi_k = \phi(k)$ is the quark gap angle related to the BCS angle θ_k by, $\tan(\phi_k - \theta_k) = m/k$, and $\omega_k = k e^{-2\Theta_k}$ is the effective gluon self energy. The quark gap equation is UV finite for the linear potential, $-8\pi\sigma/p^4$, but not for the Coulomb potential, $-4\pi\alpha_s/p^2$. The gluon gap equation has both logarithmical and quadratical UV divergences and an integration cutoff, $\Lambda = 4$ GeV, determined in previous studies is used in both equations. The gap equations yield the quark, $E_k = \sqrt{M(k)^2 + k^2} = M(k)/\sin\phi_k$, and gluon, ω_k , self-energies from which the dressed (constituent) quasi-particle masses can be extracted at zero momentum: $M_u(0) \cong 125$ MeV, $M_g(0) = \omega(0) \cong 800$ MeV. The gap angles also determine the quark, $\langle q\bar{q} \rangle = \langle \Omega | \bar{\Psi}(0) \Psi(0) | \Omega \rangle = -(177 \text{ MeV})^3$, and gluon, $\langle \alpha G_{\mu\nu}^a G_a^{\mu\nu} \rangle = (433 \text{ MeV})^4$, condensates which are in reasonable agreement with QCD sum rule, $-(236 \text{ MeV})^3$, and lattice, $(441 \text{ MeV})^4$, values, respectively.

4. Meson and glueball states

Turning to excited states, the lightest in the quark and gluon sectors are two-body mesons ($q\bar{q}$) and glueballs (gg). The meson states were calculated using both the TDA and RPA, the latter being essential to preserve chiral symmetry. The TDA and RPA states are respectively, $|\Psi_{TDA}^{nJPC}\rangle = Q_{nJPC}^\dagger(TDA)|\Omega\rangle$, $|\Psi_{RPA}^{nJPC}\rangle = Q_{nJPC}^\dagger(RPA)|\Omega_{RPA}\rangle$, with J , the total angular momentum, P , the parity, C , the C -parity, n , the radial-node quantum number and

$$Q_{nJPC}^\dagger(TDA) = \int \frac{d\mathbf{k}}{(2\pi)^3} \Psi_{\mu\bar{\mu}}^{nJPC}(\mathbf{k}) B_\mu^{C\dagger}(\mathbf{k}) D_{\bar{\mu}}^{C\dagger}(-\mathbf{k}) \quad (23)$$

$$Q_{nJPC}^\dagger(RPA) = \int \frac{d\mathbf{k}}{(2\pi)^3} [X_{\mu\bar{\mu}}^{nJPC} B_\mu^{C\dagger}(\mathbf{k}) D_{\bar{\mu}}^{C\dagger}(-\mathbf{k}) - Y_{\mu\bar{\mu}}^{nJPC} B_\mu^C(\mathbf{k}) D_{\bar{\mu}}^C(-\mathbf{k})]. \quad (24)$$

Note the RPA now involves the RPA vacuum defined by $Q_{nJPC}(RPA)|\Omega_{RPA}\rangle = 0$. The TDA and coupled RPA equations are given in Refs. [1, 2]. For the vector mesons ρ , J/ψ , the wavefunctions have been generalized to include both s and d waves leading to four coupled RPA equations detailed in Ref. [3].

Exactly solving the TDA and RPA equations of motion, $H_{CG}|\Psi^{nJPC}\rangle = M_{nJPC}|\Psi^{nJPC}\rangle$, yields predictions for the u/d , s , c and b meson spectra in reasonable agreement with observation. Several results are especially noteworthy. Except for the pion and light η , the TDA and RPA spectra were essentially identical. For light mesons, a realistic pion mass (≈ 150 MeV) was obtained along with Regge trajectories that were also consistent with scattering measurements, $J = \alpha(t) = bt + \alpha(0) \approx .9t + .5$, $t = M_{nJPC}^2$. For heavy mesons, the predicted small hyperfine splittings were in excellent agreement with data as summarized in Table 1. Further, the CG model accurately predicted [3] the lightest bottomonium state years before its discovery [4] and much closer than both lattice [5] and non-relativistic QCD [6] results.

Table 1: Model comparison of heavy meson predictions with data.

in MeV	NRQCD	lattice	Coulomb gauge	data
$\eta_c - J/\Psi$	104	90	125	117.7
$\eta_b - \Upsilon$	39 [†]	61 [†]	70 [†]	71.4
m_{η_b}	9421 \pm 11 [†]	9409 [†]	9395	9389

[†] predicted before pseudoscalar bottomonium discovery

It is significant that the CG model is able to simultaneously describe the small charmonium/bottomonium and large π/ρ splittings with the same hyperfine interaction. This is possible because the RPA meson operator commutes with the chiral charge, $Q_5 = \int d\mathbf{x} \Psi^\dagger(\mathbf{x}) \gamma_5 \Psi(\mathbf{x})$, and preserves chiral symmetry yielding a light Goldstone pion. Conversely, the TDA operator does not commute and the TDA pion for the same H_{CG} has mass about 500 MeV. Hence chiral symmetry is predominantly responsible for the large π/ρ splitting, contributing about 400 MeV. Note that the model also describes the excited state

spin splittings, typically less than 200 MeV, which are entirely from the hyperfine interaction. These states are not governed by chiral symmetry and the TDA and RPA results agree to within a few percent. See Ref. [3] for a more detailed discussion of model meson results.

In the gluonic sector, the TDA glueball wavefunction for two constituent gluons is given by

$$|\Psi_{LS}^{JPC}\rangle = \int \frac{d\mathbf{k}}{(2\pi)^3} \Phi_{LS\lambda_1\lambda_2}^{JPC}(\mathbf{k}) \alpha_{\lambda_1}^{a\dagger}(\mathbf{k}) \alpha_{\lambda_2}^{a\dagger}(-\mathbf{k}) |\Omega\rangle . \quad (25)$$

Here L is the orbital angular momentum and $S = 0, 1$ or 2 is the total intrinsic gluon spin. Using this quasiparticle basis the excited glueball spectrum was computed by diagonalizing the Hamiltonian in the TDA truncated at the 1p-1h quasiparticle level. The RPA spectrum was also calculated and agreed with the TDA to within 1 per cent. The predicted $J^{PC} = 0^{\pm+}, 2^{\pm+}$ and 3^{++} states agree well with quenched lattice gauge measurements. The predicted $J^{PC} = 2^{++}, 4^{++}$ glueballs yielded a Regge trajectories close to the observed pomeron result, $\alpha_P \approx .25t + 1$. See Ref. [7] for further details.

5. Oddball and hybrid meson states

Predictions for the low lying spectra of ggg glueballs and $q\bar{q}g$ hybrid mesons are now presented and discussed. Since these hadrons consist of 3 constituents, the masses for selected J^{PC} states are computed variationally

$$M_{JPC} = \frac{\langle \Psi^{JPC} | H_{CG} | \Psi^{JPC} \rangle}{\langle \Psi^{JPC} | \Psi^{JPC} \rangle} . \quad (26)$$

The variational approximation has been comprehensively tested in two body systems by comparison with exact diagonalization and found to be accurate to a few percent. For $C = -1$ glueballs (oddballs), Fock states with at least 3 gluons are necessary and the wavefunction is ($\mathbf{q}_{i=1,2,3}$ are cm gluon momenta)

$$|\Psi^{JPC}\rangle = \int d\mathbf{q}_1 d\mathbf{q}_2 d\mathbf{q}_3 \delta(\mathbf{q}_1 + \mathbf{q}_2 + \mathbf{q}_3) F_{\mu_1\mu_2\mu_3}^{JPC}(\mathbf{q}_1, \mathbf{q}_2, \mathbf{q}_3) C^{abc} \alpha_{\mu_1}^{a\dagger}(\mathbf{q}_1) \alpha_{\mu_2}^{b\dagger}(\mathbf{q}_2) \alpha_{\mu_3}^{c\dagger}(\mathbf{q}_3) |\Omega\rangle . \quad (27)$$

The color tensor, C^{abc} , is either antisymmetric, f^{abc} , for $C = 1$ or symmetric, d^{abc} , for $C = -1$ and Boson statistics requires $C = -1$ oddballs to have a symmetric space-spin wavefunction. Using a two-parameter variational radial wavefunction, the J^{--} oddball states have been calculated. The hyperfine interaction, H_{gg} , was suppressed and only the Abelian component of the magnetic fields was included. The Monte Carlo method with the adaptive sampling algorithm VEGAS was used and numerical convergence required between 10^5 and 10^6 samples. In Table 2 results [8] are compared to lattice gauge results [9, 10] and a Wilson-loop inspired model [11]. The oddball mass sensitivity to both statistical and variational uncertainties was a few per cent.

Table 2: Oddball quantum numbers and masses in MeV. Error (Monte Carlo) for H_{CG} is less than 100 MeV, lattice errors are typically 200-300 MeV.

Model	1^{--}	3^{--}	5^{--}	7^{--}
Coulomb gauge [8]	3950	4150	5050	5900
lattice [9]	3850	4130		
lattice [10]	3100	4150		
Wilson-loop [11]	3490	4030		

The predicted oddball Regge trajectories from several approaches are displayed in Fig. 1. Constituent gluon predictions are represented by boxes, solid triangles and solid circles and correspond to a Wilson-loop inspired potential model [11], a simpler harmonic oscillator calculation [8] and the Coulomb gauge model [8], respectively. Lattice results are depicted by open circles [9] and diamonds [10]. The odderon trajectories for the harmonic oscillator and Coulomb gauge models are represented respectively by the solid lines, $\alpha_O^M = 0.18t + 0.25$ and $\alpha_O^{CG} = 0.23t - 0.88$, while the ω trajectory is the much steeper dashed line.

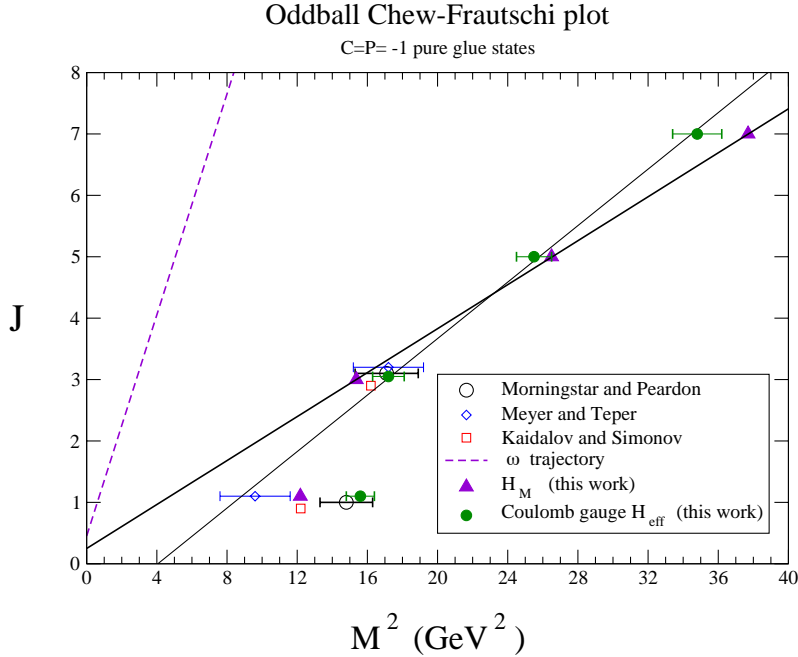


Figure 1: Comparison of the ω meson Regge trajectory to odderon trajectories from constituent gluon models and lattice.

Three key results follow which are also supported by a more recent, but simpler constituent gluon model [12]. First, the odderon starts with the 3^{--} state and not the 1^{--} which is on a daughter trajectory. Note that there are no lattice 5^{--} glueball predictions which are necessary to confirm this point and we strongly recommend that future studies calculate higher J^{--} states. Second, all approaches predict the 3^{--} mass is near 4 GeV. Third, the predicted odderon has slope similar to the pomeron but intercept clearly lower than the ω value. This provides an explanation for why the odderon has not been observed in total cross section data which is predominantly governed by the larger ω intercept. Future searches should therefore focus on differential cross section measurements, $d\sigma/dt$, at large t where the odderon trajectory dominates.

Turning to the hybrid meson system, the non-abelian magnetic field terms are now included. For a $q\bar{q}g$ hybrid the color structure is given by $SU_c(3)$ algebra, $(3 \otimes \bar{3}) \otimes 8 = (8 \otimes 8) \oplus (8 \otimes 1) = 27 \oplus 10 \oplus 10 \oplus 8 \oplus 8 \oplus 1$. Note to obtain an over all color singlet the quarks must be in an octet state, like the gluon, which produces a repulsive $q\bar{q}$ interaction, confirmed by lattice at short range, that raises the mass of the hybrid meson. Denoting the momenta of the dressed quark, anti-quark and gluon by \mathbf{q} , $\bar{\mathbf{q}}$ and \mathbf{g} , respectively, the hybrid cm system wavefunction is

$$|\Psi^{JPC}\rangle = \int d\mathbf{q}d\bar{\mathbf{q}}d\mathbf{g}\delta(\mathbf{q} + \bar{\mathbf{q}} + \mathbf{g})\Phi_{\lambda\lambda\mu}^{JPC}(\mathbf{q}, \bar{\mathbf{q}}, \mathbf{g})T_{c\bar{c}}^a B_{\lambda C}^\dagger(\mathbf{q})D_{\lambda\bar{c}}^\dagger(\bar{\mathbf{q}})\alpha_\mu^{a\dagger}(\mathbf{g})|\Omega\rangle. \quad (28)$$

With two variational parameters, the hybrid mass was computed using the Monte Carlo method which required about 50 million samples for convergence with error around ± 50 MeV. The predicted [13] low lying mass spectra for light hybrid mesons, with both conventional and unconventional (labeled exotica) quantum numbers, are presented in Fig. 2. Note the isospin splitting due to

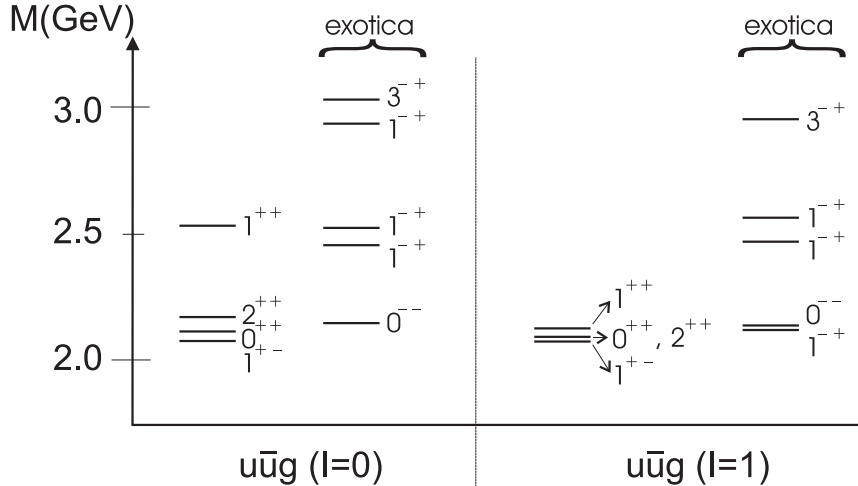


Figure 2: Low lying isoscalar and isovector $u\bar{u}g$ spectra.

quark annihilation (only in the $I = 0$ channel) which increases the hybrid mass. The most significant result is that all hybrid masses, especially the lightest exotic 1^{-+} state, are above 2 GeV. As summarized in Fig. 3, this is consistent with lattice [14, 15] and Flux Tube model [16] results and strongly suggests that the 1^{-+} $\pi(1600)$, and more clearly observed $\pi(1400)$, are not hybrid meson states.

$u\bar{d}g$ Hybrid Meson

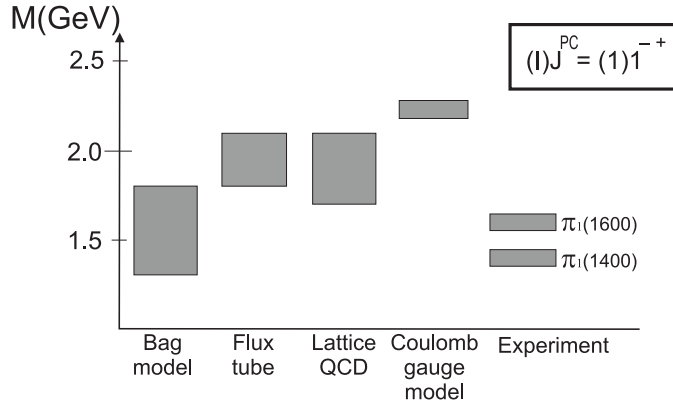


Figure 3: Confrontation of different hybrid meson models with data.

The strange $s\bar{s}g$ and charmed $c\bar{c}g$ hybrid spectra are illustrated in Fig. 4. Due to the hyperfine interaction, the $c\bar{c}g$ spectra has a slightly different level ordering than the $u\bar{u}g$ and $s\bar{s}g$ results. The $s\bar{s}g$ and $c\bar{c}g$ exotic 1^{-+} states are also in reasonable agreement with both lattice and Flux Tube results.

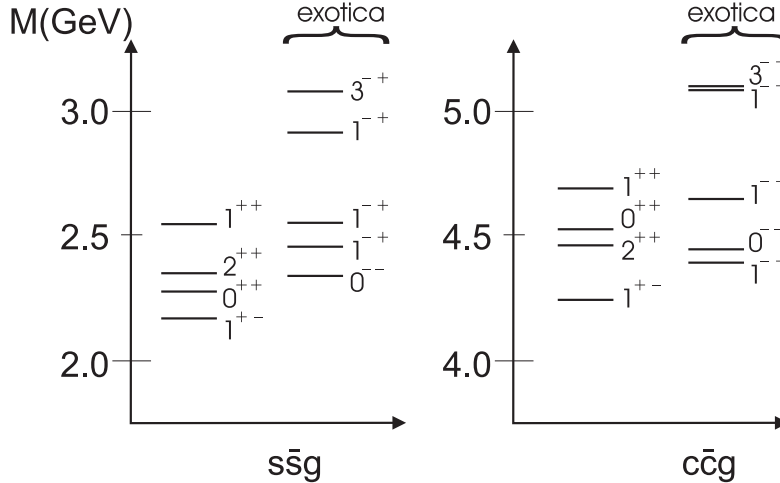


Figure 4: Selected low lying $s\bar{s}g$ and $c\bar{c}g$ spectra.

6. Tetraquark states

As illustrated in Fig. 5, the $SU_c(3)$ color algebra for four quarks produces 81 color states, $3 \otimes \bar{3} \otimes 3 \otimes \bar{3} = 27 \oplus 10 \oplus \bar{10} \oplus 8 \oplus 8 \oplus 8 \oplus 8 \oplus 1 \oplus 1$. Two are color singlets that can be obtained in four different ways depending on the intermediate color coupling: singlet scheme, non-exotic meson-meson molecule, and three exotic atoms, one octet and two diquark schemes involving the triplet and the sextet representations. The two color singlets, $\delta_{c_1 c_2} \delta_{c_3 c_4}$ and $\delta_{c_1 c_4} \delta_{c_3 c_2}$,

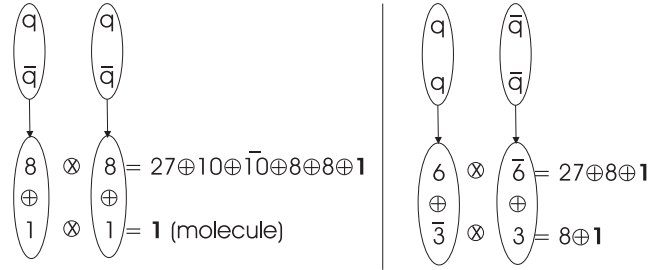


Figure 5: Color singlets from four different representations.

are linearly independent and form a color space as depicted in Fig. 6 with the first along the horizontal axis and the second, in the limit of large N_c , vertical. For physical $N_c = 3$ they are not orthogonal, as the second is now rotated with respect to the first held fixed. However they still span the entire color space so that any of the four schemes can be represented as a linear combination of the two singlets. This means that the color degree of freedom does not forbid a tetraquark transition into two mesons.

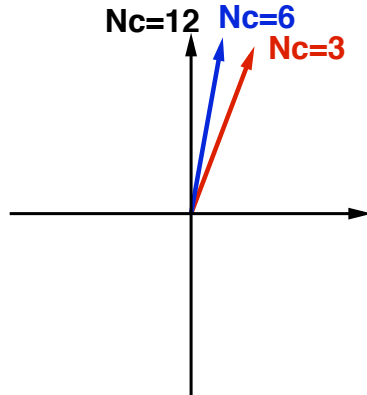


Figure 6: Color space.

Denoting the momenta of the quarks by \mathbf{q}_1 , \mathbf{q}_3 , and those of the anti-quarks by \mathbf{q}_2 , \mathbf{q}_4 , the cm tetraquark wavefunction is

$$|\Psi^{JPC}\rangle = \int d\mathbf{q}_1 d\mathbf{q}_2 d\mathbf{q}_3 d\mathbf{q}_4 \delta(\mathbf{q}_1 + \mathbf{q}_2 + \mathbf{q}_3 + \mathbf{q}_4) \Phi_{\lambda_1 \lambda_2 \lambda_3 \lambda_4}^{JPC}(\mathbf{q}_1, \mathbf{q}_2, \mathbf{q}_3, \mathbf{q}_4) R_{C_3 C_4}^{C_1 C_2} B_{\lambda_1 C_1}^\dagger(\mathbf{q}_1) D_{\lambda_2 C_2}^\dagger(\mathbf{q}_2) B_{\lambda_3 C_3}^\dagger(\mathbf{q}_3) D_{\lambda_4 C_4}^\dagger(\mathbf{q}_4) |\Omega\rangle, \quad (29)$$

where the color elements, $R_{C_3 C_4}^{C_1 C_2}$, depend on the specific color scheme chosen. Contributions to the Hamiltonian expectation value involve 4 self-energy, 6 scattering, 4 annihilation and 70 exchange terms each of which can be reduced to 12 dimensional integrals that are evaluated in momentum space. Again, these were computed [17] by performing Monte Carlo calculations (typically 50 million samples) and the hyperfine interaction was not included. The meson-meson molecule yields the lightest mass state for a given J^{PC} which is due to cancellation of certain interactions by color factors in the singlet-singlet molecular representation and also the presence of repulsive forces in the other, more exotic, color schemes. The ground state is a non-exotic 1^{++} with mass around 1.2 GeV. The remaining low lying spectra for states having both conventional and unconventional (loosely labeled exotica but not exotic) quantum numbers in the molecular singlet color representation is displayed in Fig. 7. As in the hybrid calculation, there are isospin splitting contributions, up to several hundred MeV, but only in the octet scheme (not shown) from quark annihilation interactions ($q\bar{q} \rightarrow g \rightarrow q\bar{q}$) in the $I_{q\bar{q}} = 0$ channel. The annihilation interaction is repulsive, yielding octet states with $I = 2$ lower than the $I = 1$ which are lower than the $I = 0$. The meson-meson states are all isospin degenerate producing several molecular tetraquark states with the same J^{PC} in the 1 to 2 GeV

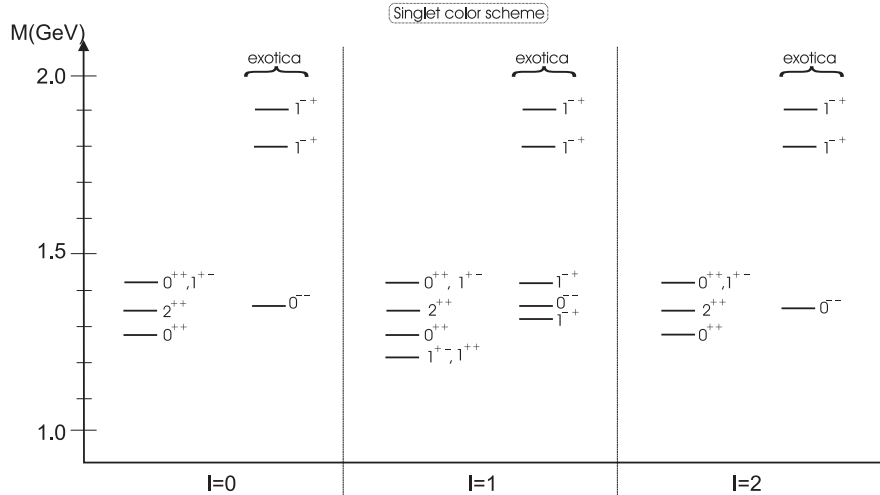


Figure 7: Non-exotic tetraquark color singlet (molecule) spectra.

region. The $I = 1$ and 2 states can be observed in different electric charge channels (different I_z) at about the same energy, which is a useful experimental signature. Most important, the predicted lightest 1^{-+} is at 1.32 GeV, near the observed $\pi(1400)$, suggesting this state has a non-exotic meson-meson resonance molecular structure. Indeed, the predicted tetraquark mass for all exotic 1^{-+} states in the octet color configurations is above 2 GeV. This is consistent with the model predictions, discussed in the previous section, for exotic hybrid meson 1^{-+} states also lying above 2 GeV due to repulsive octet color quark interactions. Note that C parity forbids exotic diquark ($[3 \otimes 3] \otimes [\bar{3} \otimes \bar{3}]$) states in the 1^{-+} channel. The other J^{PC} states in both the triplet and the sextet diquark color representations also have computed masses (not shown) heavier than in the singlet representation and comparable to the octet scheme results. Since there are two linearly independent color configurations, in lieu of a color mixing calculation that would order the eigenvalues for a given basis, the variational procedure requires accepting as the best approximation to the physical states the molecular scheme as the lightest along with the heavier linear combination that is orthogonal.

Finally, the important issue of meson and tetraquark mixing is addressed [18] for the $J^{PC} = 0^{\pm+}$ and 1^{-} states. Using the notation, $|q\bar{q}\rangle$ and $|q\bar{q}q\bar{q}\rangle$ for $|\Psi^{J^{PC}}\rangle$, the mixed state is given by $|J^{PC}\rangle = a|n\bar{n}\rangle + b|s\bar{s}\rangle + c|n\bar{n}n\bar{n}\rangle + d|n\bar{n}s\bar{s}\rangle$, where $n\bar{n} = \frac{1}{\sqrt{2}}(u\bar{u} + d\bar{d})$. The state $|s\bar{s}s\bar{s}\rangle$ is not included since its mass is much higher. The coefficients a, b, c and d are determined by diagonalizing the Hamiltonian matrix. The off-diagonal mixing element, $M = \langle q\bar{q}|H_C^{\text{CG}}|q\bar{q}q\bar{q}\rangle$, only involves H_C^{CG} which connects meson and tetraquark states. Of the six off-diagonal matrix elements two, $\langle s\bar{s}|H_C^{\text{CG}}|n\bar{n}\rangle$ and $\langle s\bar{s}|H_C^{\text{CG}}|n\bar{n}n\bar{n}\rangle$, vanish and one, $\langle n\bar{n}n\bar{n}|H_C^{\text{CG}}|n\bar{n}s\bar{s}\rangle$, is computed very small. The remaining three elements are, $\langle n\bar{n}|H_C^{\text{CG}}|n\bar{n}n\bar{n}\rangle$, $\langle n\bar{n}|H_C^{\text{CG}}|n\bar{n}s\bar{s}\rangle$ and $\langle s\bar{s}|H_C^{\text{CG}}|n\bar{n}s\bar{s}\rangle$. Because of color factors, nonzero mixing only exists for $q\bar{q}$ annihilation between different singlet $q\bar{q}$ clusters. There are two contributions to each mixing matrix element. One is

$$M_1 = \frac{1}{2} \int d\mathbf{q}_1 d\mathbf{q}_2 d\mathbf{q}_3 V(k) \mathcal{U}_{\lambda_1}^\dagger(\mathbf{q}_1) \mathcal{U}_{\lambda_1'}(-\mathbf{q}_4) \quad (30)$$

$$\mathcal{U}_{\lambda_3}^\dagger(\mathbf{q}_3) \mathcal{V}_{\lambda_2}(\mathbf{q}_2) \Phi_{\lambda_1 \lambda_2 \lambda_3 \lambda_4}^{J^{PC\dagger}}(\mathbf{q}_1, \mathbf{q}_2, \mathbf{q}_3) \Phi_{\lambda_1' \lambda_4}^{J^{PC}}(-2\mathbf{q}_4),$$

with $V(k)$ the confining potential, $\mathbf{q}_4 = -\mathbf{q}_1 - \mathbf{k}$, $\mathbf{k} = \mathbf{q}_2 + \mathbf{q}_3$ and

$$\mathcal{U}_\lambda = \frac{1}{\sqrt{2}} \begin{pmatrix} \sqrt{1+s_q} \\ \sqrt{1-s_q} \sigma \cdot \hat{\mathbf{q}} \end{pmatrix} \chi_\lambda \quad (31)$$

$$\mathcal{V}_\lambda = \frac{1}{\sqrt{2}} \begin{pmatrix} -\sqrt{1-s_q} \\ \sqrt{1+s_q} \sigma \cdot \hat{\mathbf{q}} \end{pmatrix} \chi_\lambda, \quad (32)$$

are dressed, BCS spinors. Again $s_q = \sin \phi_q$ is obtained from the gap equation solution. The other contribution has the form

$$M_2 = \frac{1}{2} \int d\mathbf{q}_1 d\mathbf{q}_2 d\mathbf{q}_3 V(k) \mathcal{V}_{\lambda_4}^\dagger(\mathbf{q}_4) \mathcal{V}_{\lambda_4'}(-\mathbf{q}_1) \quad (33)$$

$$\mathcal{U}_{\lambda_3}^\dagger(\mathbf{q}_3) \mathcal{V}_{\lambda_2}(\mathbf{q}_2) \Phi_{\lambda_1 \lambda_2 \lambda_3 \lambda_4}^{J^{PC\dagger}}(\mathbf{q}_1, \mathbf{q}_2, \mathbf{q}_3) \Phi_{\lambda_1 \lambda_4}^{J^{PC}}(2\mathbf{q}_1).$$

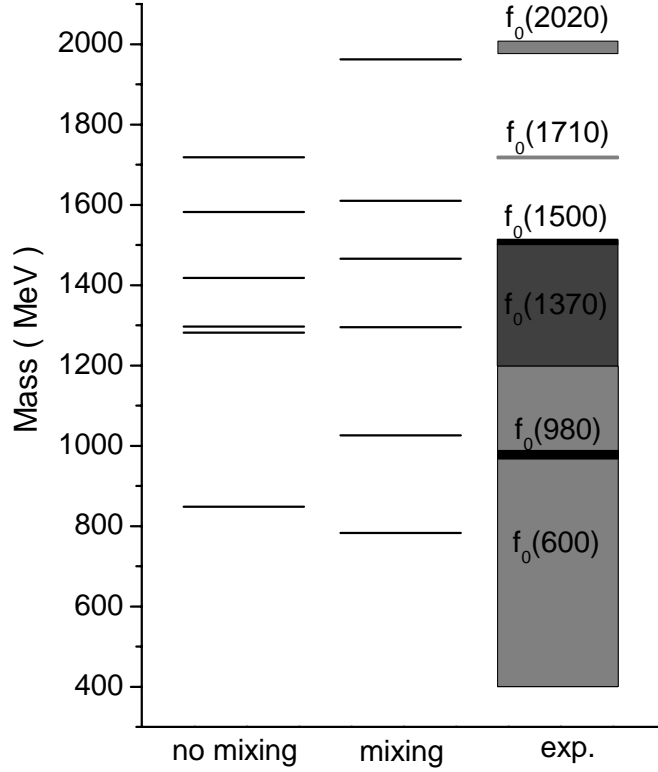


Figure 8: Unmixed and mixed f_0 spectrum compared to data.

Because new model masses are computed, the unmixed variational basis states need not be ones producing a minimal, unmixed mass. This allows adjusting one of the two variational parameters, denoted by γ , to provide an optimal variational mixing prediction. For 0^{++} states, the mixing term vanishes for $\gamma = 0$ and then increases with increasing γ . For the optimum variational value, $\gamma = 0.2$, the matrix elements are $\langle s\bar{s}|H_C^{CG}|n\bar{n}s\bar{s}\rangle = 365$ MeV, $\langle n\bar{n}|H_C^{CG}|n\bar{n}n\bar{n}\rangle = 166$ MeV and $\langle n\bar{n}|H_C^{CG}|n\bar{n}s\bar{s}\rangle = 45$ MeV. With the calculated matrix elements and unmixed meson and tetraquark masses, the complete Hamiltonian matrix was diagonalized to obtain the expansion coefficients and masses for the corresponding eigenstates illustrated in Fig. 8. Mixing clearly provides an improved description for the f_0 spectrum as the σ meson mass is lowered from 848 MeV to 776 MeV, the strange scalar meson mass decreases from 1297 MeV to 1006 MeV, closer to the observed value of 980 MeV, and the other f_0 states are now also in better agreement with data. Including chiral symmetry corrections, which are

omitted by the TDA variational basis states, will further lower the σ prediction, closer to the now accepted value of 450 MeV [19]. The mixing coefficients also provide new structure insight, predicting the $\sigma/f_0(600)$ is predominantly a mixture of $n\bar{n}$ and $n\bar{n}n\bar{n}$ states while the $f_0(980)$ is mainly $s\bar{s}$ and $n\bar{n}s\bar{s}$ states. This is consistent with the growing consensus that the $\sigma/f_0(600)$ state is a $\pi\pi$ resonance (pole in the $\pi\pi$ scattering amplitude) with a molecular tetraquark nature. Future mixing calculations will include both scalar glueballs and hybrid mesons which should further improve describing the high lying f_0 spectrum, anticipated to have a few newly discovered states, and also aid identification of gluonic states.

For 0^{-+} states, the value $\gamma = 0.5$ yields reasonable η and η' masses with mixing elements $\langle n\bar{n}|H_C^{\text{CG}}|n\bar{n}n\bar{n}\rangle = 219$ MeV, $\langle n\bar{n}|H_C^{\text{CG}}|n\bar{n}s\bar{s}\rangle = 157$ MeV and $\langle s\bar{s}|H_C^{\text{CG}}|n\bar{n}s\bar{s}\rangle = 138$ MeV. The unmixed η , η' masses changed from 610 MeV, 1002 MeV to 531 MeV, 970 MeV, respectively, both closer to the observed values of 547.51 MeV and 957.78 MeV.

A novel mixing result was obtained for the 1^{--} states. Again the mixing matrix elements were 0 for $\gamma = 0$ but, and very interesting, also essentially 0 for all values of γ . The Coulomb gauge model therefore predicts minimal flavor mixing for vector mesons which agrees with the known, predominantly ideal, ω/ϕ mixing. Related, the model still provides a good vector meson spectrum description since the unmixed $n\bar{n}$ and $s\bar{s}$ states were already in agreement [3] with observation.

7. Summary

Concluding, the Coulomb gauge model provides a comprehensive, unified quark-gluon framework for realistically describing the vacuum and meson spectrum and also agrees with glueball and hybrid meson predictions from alternative approaches. The model is sufficiently robust, as evidenced by accurately predicting the η_b mass and attending hyperfine splitting, to guide experimentalists in future particle searches, especially states with explicit gluonic degrees of freedom. Further, this approach retains the attractive wavefunction picture, not available through lattice QCD, which provides deeper hadronic insight that should be helpful in understanding states with unconventional quantum numbers like the observed π_1 which appears to be a meson-meson resonance. Finally, the approach is amendable to further refinements through improved confining interactions and extended model spaces involving additional quasiparticle Fock states.

Acknowledgments

Thanks to the NAPP2010 organizers, especially B. Vlahovic and I. Supek. I. General and P. Wang are gratefully acknowledged. Support is from grants U. S. DOE DE-FG02-03ER41260, FPA 2008-00592, FIS2008-01323 plus 227431, Hadron-Physics2 (EU) and PR34-1856-BSCH, UCM-BSCH GR58/08, 910309 and PR34/07-15875.

References

- [1] F. J. Llanes-Estrada and S. R. Cotanch, Phys. Rev. Lett. **84** (2000) 1102.
- [2] F. J. Llanes-Estrada and S. R. Cotanch, Nucl. Phys. A **697** (2002) 303.
- [3] F. J. Llanes-Estrada et al., Phys. Rev. C **70** (2004) 035202.
- [4] B. Aubert et al., Phys. Rev. Lett. **101** (2008) 071801.
- [5] X. Liao and T. Manke, Phys. Rev. D **65** (2002) 074508.
- [6] B. A. Kniehl et al., Phys. Rev. Lett. **92** (2004) 242001.
- [7] F. J. Llanes-Estrada et al., Nucl. Phys. A **710** (2002) 45.
- [8] F. J. Llanes-Estrada, P. Bicudo and S. R. Cotanch, Phys. Rev. Lett. **96** (2006) 081601.
- [9] C. J. Morningstar and M. Peardon, Phys. Rev. D **60** (1999) 034509.
- [10] H. B. Meyer and M. Teper, Phys. Lett. B **605** (2005) 344.
- [11] A. B. Kaidalov and Y. A. Simonov, Phys. Lett. B **477** (2000) 163.
- [12] V. Mathieu, C. Semay and B. Silvestre-Brac, Phys. Rev. D **77** (2008) 094009.
- [13] I. J. General, F. J. Llanes-Estrada and S. R. Cotanch, Eur. Phys. J. C **51** (2007) 347.
- [14] J. N. Hedditch et al., Phys. Rev. D **72** (2005) 114507.
- [15] Y. Liu and X. Q. Luo, Phys. Rev. D **73** (2006) 054510.
- [16] F. E. Close and P. Page, Nucl. Phys. B **443** (1995) 233.
- [17] I. J. General, P. Wang, S. R. Cotanch and F. J. Llanes-Estrada, Phys. Lett. B **653** (2007) 216.
- [18] P. Wang, S. R. Cotanch and I. J. General, Eur. Phys. J. C **55** (2008) 409.
- [19] R. Garcia-Martin et al., PoS **EFT09** (2009) 052.